

DoA-LF: A Location Fingerprint Positioning Algorithm with Millimeter-Wave

Zhiqing Wei, Yadong Zhao, Xinyi Liu, Zhiyong Feng

Abstract—Location fingerprint (LF) has been widely applied in indoor positioning. However, the existing studies on LF mostly focus on the fingerprint of WiFi below 6 GHz, bluetooth, ultra wideband (UWB), etc. The LF with millimeter-wave (mmWave) was rarely addressed. Since mmWave has the characteristics of narrow beam, fast signal attenuation and wide bandwidth, etc., the positioning error can be reduced. In this paper, an LF positioning method with mmWave is proposed, which is named as DoA-LF. Besides received signal strength indicator (RSSI) of access points (APs), the fingerprint database contains direction of arrival (DoA) information of APs, which is obtained via DoA estimation. Then the impact of the number of APs, the interval of reference points (RPs), the channel model of mmWave and the error of DoA estimation algorithm on positioning error is analyzed with Cramer-Rao lower bound (CRLB). Finally, the proposed DoA-LF algorithm with mmWave is verified through simulations. The simulation results have proved that mmWave has larger path loss exponent and smaller variance of shadow fading compared with low frequency signals. Besides, accurate DoA estimation can reduce the positioning error.

Index Terms—Millimeter-Wave, Location Fingerprint, Direction of Arrival Estimation, Cramer-Rao Lower Bound

I. INTRODUCTION

With the development of mobile Internet, the location based services and applications such as mobile social networks, online maps and online-to-offline (O2O) services are developing rapidly, which makes the positioning technologies critical for modern life. The global navigation satellite system (GNSS) consisting of GPS, GLONASS, GALILEO, BDS, etc. is efficient in outdoor environment. However, in indoor environment, because satellite signal is blocked by roofs and walls of buildings, GNSS does not work, which triggers the studies on indoor positioning.

LF positioning plays an important role in complex indoor environment because it does not require line-of-sight (LOS) measurement [1]. The scenario of LF positioning is illustrated in Fig. 1. There are five APs in a specific indoor environment. The features of received signals from all APs are measures at reference points (RPs), which constitute LF database. When a device appears at a spot, it measures the features of all APs to find the RPs with similar features. Then the estimated location can be the mean of the locations of K RPs with most similar features, which is K nearest node (KNN) method.

Among LF positioning systems, WiFi fingerprint systems are most widely studied and applied in indoor positioning.

The final version of this paper is published in IEEE Access. Zhiqing Wei, Yadong Zhao, Xinyi Liu and Zhiyong Feng are with Beijing University of Posts and Telecommunications, email: {weizhiqing, zhaoyadong, xinyi, fengzy}@bupt.edu.cn.

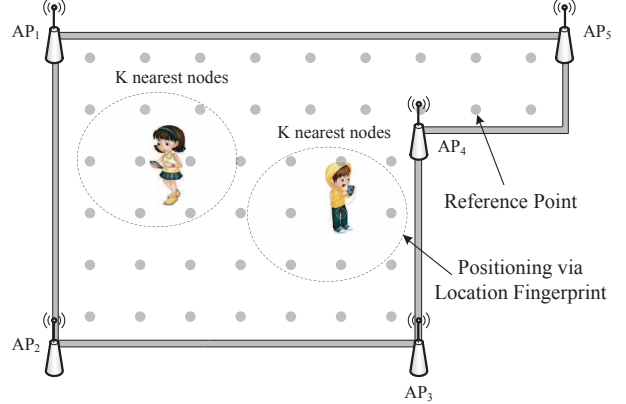


Fig. 1. The scenario of LF positioning

Except of WiFi fingerprint, UWB fingerprint systems are also studied [2][3]. Besides, with the development of bluetooth low energy (BLE) subsystem, which is “designed for machine type communication” [4], BLE devices will be more and more dense in buildings. Hence bluetooth LF based positioning is also applied in indoor positioning [5].

The schemes of LF based indoor positioning focus on the construction of radio map [6][7], the contour-based LF method [8], the gradient-based fingerprinting [9], the CSI-based indoor positioning [10][11][12] and machine learning based LF schemes [13][14], etc. As to the construction of radio map in LF positioning, Jiang *et al.* in [6] constructed radio map via crowdsourcing collection. Jung *et al.* in [7] evaluated the performance of radio map construction methods in various environments. To provide accurate LF based indoor positioning, He *et al.* in [8] developed the contour-based trilateration to combine the advantages of trilateration and fingerprinting [8]. Shu *et al.* in [9] proposed the gradient fingerprinting method to reduce the impact of varying RSSI on the accuracy of LF positioning. LF positioning schemes generally adopt RSSI information, however, the channel state information (CSI) contains more information, which can be exploited to improve the accuracy of indoor positioning. Wu *et al.* in [10] designed the fingerprinting system exploiting CSI to construct the propagation model to improve positioning accuracy. Wang *et al.* in [11] and [12] designed the CSI-based fingerprinting schemes via deep learning approach. The positioning problem is mathematically a regression problem. Besides, LF positioning methods have large amount of data in the offline database. Thus machine learning approaches can be adopted to solve the positioning problem. Mahfouz

et al. in [13] proposed a kernel-based machine learning for LF positioning. Zou *et al.* applied extreme learning machine to solve indoor positioning problem [14].

Besides the design of positioning schemes, the analysis of positioning error is also an active area. In [15], Li proposed RSSI based positioning scheme without path loss model and the Cramer-Rao lower bound (CRLB) was derived to characterize the positioning error. Naik *et al.* in [16] studied the impact of the height of AP on the positioning accuracy and the CRLB is correspondingly derived. Jin *et al.* in [17] have studied the performance of RSSI based LF positioning scheme using CRLB. And Hossain *et al.* in [18] analyzed the CRLB of signal strength difference based LF positioning scheme.

Overall, LF positioning schemes are mostly focused on the fingerprint of WiFi, Bluetooth, UWB, etc. To our best knowledge, there are rarely studies on LF positioning with mmWave. Because mmWave has the characteristics of narrow beam, fast signal attenuation and wide bandwidth, etc., mmWave signals can provide centimeter level ranging accuracy [19][20][21]. Besides, with the development of fifth generation mobile communication (5G), dense mmWave small cells will be widely deployed [22], which makes LF positioning with mmWave to be realizable. In the standard of IEEE 802.11ad, 60 GHz mmWave for multi-gigabit-per-second WiFi is developed [23]. Besides, IEEE has also started the standardization of IEEE 802.11aj, which is a WLAN system operating at 45 GHz mmWave band [24]. Thus in the near future, LF positioning with mmWave is practical.

In this paper, an LF positioning method with mmWave is proposed, which may be promising in the era of 5G when APs with mmWave are widely deployed. We utilize the characteristics of narrow beam and fast signal attenuation of mmWave to reduce positioning error. The proposed LF positioning scheme is called DoA-LF, because the fingerprint database contains DoA information of APs besides RSSI information, which is obtained via DoA estimation. Then we select K candidate RPs with the most similar features and calculate their weighted mean through weighted K nearest neighbor (WKNN) algorithm, which is the final estimated location. It is noted that the value of K has an impact on the positioning error and there exists an optimal K that can minimize the positioning error. With DoA information of APs operating on mmWave spectrum band, the positioning error is significantly reduced compared with LF positioning with signal below 6 GHz. Then the impact of the number of APs, the interval of RPs, the variance of DoA estimation, the path loss exponent and the shadow fading of mmWave on the positioning error is analyzed via Cramer-Rao Lower Bound (CRLB). Finally, the analysis results are verified by simulation results. The key parameters and notations in this paper are listed in Table I.

The rest of this paper is organized as follows. In Section II, system model is introduced. Section III presents the proposed DoA-LF algorithm. In Section IV, CRLB is achieved, which yields the impact of various parameters on the positioning error. Simulation results are provided in Section V to verify our scheme and analysis results. Finally, Section VI summarizes this paper.

TABLE I
KEY PARAMETERS AND NOTATIONS

Symbol	Description
$PL(d)$	Path loss at a distance d
n	Path loss exponent
X_σ	Shadow fading factor
(\hat{x}, \hat{y})	Estimated location coordinates
(x_i, y_i)	Location coordinates of i th RP
\mathbf{s}	Signal strength vector
φ	Angle vector
Q	Number of APs
M	Number of RPs
A	Test area
θ	Location of the test point
r	Location of the estimated point
$\Pr(r \theta)$	Conditional probability
$d_{r\theta}$	Euclidean distance between r and θ
d_{ir}	Euclidean distance between r and i th AP
$d_{i\theta}$	Euclidean distance between θ and i th AP
$s_{i\theta}$	Actual signal strength of i th AP at the test point
s_{ir}	Received signal strength of the i th AP at point r
$\varphi_{i\theta}$	DoA of i th AP at the test point
φ_{ir}	DoA of the i th AP at point r
σ_s^2	Variance of received signal strength
σ_φ^2	Variance of DoA estimation
$J(\hat{\theta})$	Fisher Information Matrix
$C_{\hat{\theta}}$	Cramer-Rao Lower Bound
AP	Access point
RP	Reference point
TP	Test point
LF	Location fingerprint
RSSI	Received signal strength indicator

II. SYSTEM MODEL

The 60 GHz mmWave is adopted for multi-gigabit-per-second WiFi [23]. Hence 60 GHz mmWave is adopted in LF positioning. In this section, the channel model of 60 GHz mmWave and the process of LF positioning are presented.

A. 60 GHz mmWave Channel Model

The channel model of 60 GHz mmWave is [25][26]

$$PL(d)[dB] = PL(d_0) + 10n \log\left(\frac{d}{d_0}\right) + X_\sigma, d > d_0, \quad (1)$$

where $PL(d_0) = 20 \log\left(\frac{4\pi d_0}{\lambda}\right)$ is free-space path loss at a reference distance d_0 , which is generally set as $d_0 = 1$ m. The path loss exponent is n . X_σ is the shadow fading factor modeled by a Gaussian random variable with mean zero and variance σ_s^2 .

In DOA-LF algorithm, besides RSSI information, DoA information is also needed, which can be obtained via multiple signal classification (MUSIC) algorithm. Since MUSIC algorithm is well known in the area of array signal processing, we do not introduce MUSIC algorithm in this paper. Readers can refer to [31] for details. The MUSIC algorithm has lower computational complexity compared with other DoA algorithms. However, other DoA algorithms can also be adopted besides MUSIC algorithm. If a DoA algorithm has small error, the performance of positioning algorithm can be correspondingly improved.

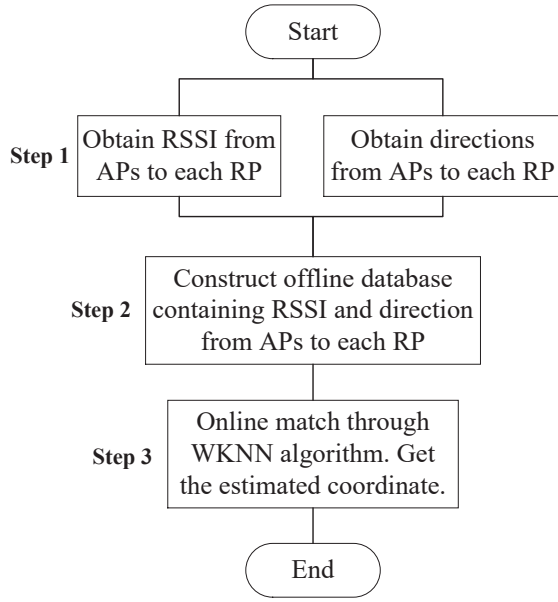


Fig. 2. The proposed DoA-LF algorithm.

B. DoA-LF Positioning Algorithm

LF positioning plays an important role in complex indoor environment. LF positioning algorithm consists of two steps, namely, offline database construction and online matching. Weighted K nearest neighbor (WKNN) algorithm is widely applied in LF positioning [32][33][34], where the weighted mean of the coordinates of K nearest RPs is calculated as the estimated coordinates. The weight coefficient w_i is generally inversely proportional to the Euclidean distance between the estimated point and i th RP [32][33] in the feature space spanning by the vectors containing RSSI and DoA information. Hence the estimated coordinates are as follows [32][33].

$$w_i = \frac{\gamma}{d_i + \varepsilon},$$

$$(\hat{x}, \hat{y}) = \frac{\sum_{i=1}^K w_i(x_i, y_i)}{\sum_{i=1}^K w_i}, \quad (2)$$

where d_i is the Euclidean distance in the feature space between the measured point and the i th RP. (\hat{x}, \hat{y}) are the estimated coordinates and (x_i, y_i) are the coordinates of i th RP. γ is normalized parameter and ε is a small positive number in order to prevent the denominator being zero.

III. THE PROPOSED DOA-LF ALGORITHM

In this section, the characteristics of mmWave, such as narrow beam and fast attenuation, are exploited to construct an LF positioning algorithm called DoA-LF algorithm. The DoA information of APs obtained by MUSIC algorithm is combined with the RSSI of APs to construct a new offline database for online matching. Then WKNN algorithm is adopted to calculate the estimated coordinates. Fig. 2 illustrates the process of proposed DoA-LF algorithm.

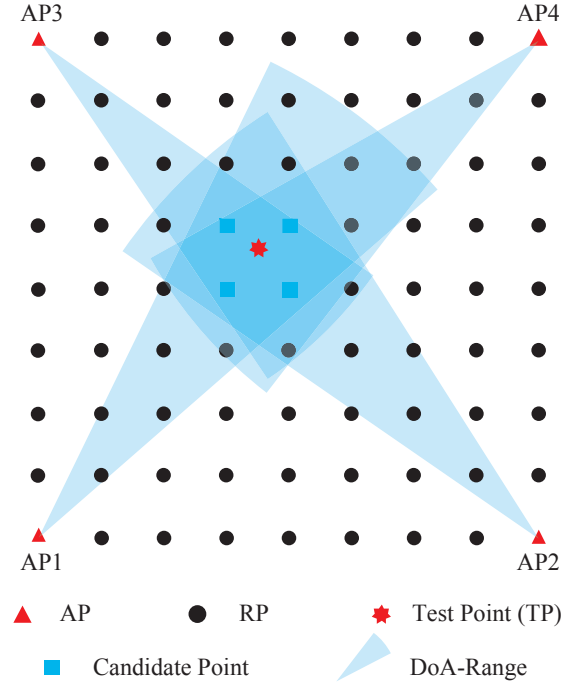


Fig. 3. A scenario of proposed DoA-LF positioning.

Step 1: Obtain RSSI and DoA information from APs to each RP.

Q APs and M RPs are deployed in a specific area, which is illustrated in Fig. 3. The RSSIs of APs at each RP are measured, which are saved in a vector $\mathbf{s}_i = [s_{1i}, s_{2i}, \dots, s_{Qi}]$ with $s_{ji}, j = 1, \dots, Q$ denoting the RSSI of j th AP at i th RP.

Meanwhile, the MUSIC algorithm is adopted for DoA estimation. The directions of APs at each RP are measured, which are saved in a vector $\boldsymbol{\varphi}_i = [\varphi_{1i}, \varphi_{2i}, \dots, \varphi_{Qi}]$ with $\varphi_{ji}, j = 1, \dots, Q$ denoting the DoA of j th AP at i th RP. It is noted that the RSSI and DoA information is obtained simultaneously.

Step 2: Construct offline database.

Combining Q -dimensional RSSI vector and Q -dimensional direction vector, we obtain $2Q$ -dimensional vector $[\mathbf{s}_i, \boldsymbol{\varphi}_i]$ representing the features of i th RP. The vectors of all RPs span a feature space and construct the offline database for DoA-LF positioning with mmWave.

Step 3: Online matching.

Comparing RSSI and direction information of test point with the data in offline database, we can find out K nearest RPs whose features are closest to test point. Then we calculate the estimated coordinates via the weighted mean of K nearest RPs using (2).

For example, in Fig. 3, there are 4 APs and 77 RPs in an area. Firstly, an offline database is established, which consists of RSSI and DoA information of all RPs. Secondly, $K = 4$ candidate RPs with the most similar features are selected, which are denoted by the squares in Fig. 3. Finally, the estimated coordinates can be obtained via calculating the weighted mean of the selected $K = 4$ candidate RPs.

IV. ANALYSIS OF POSITIONING ERROR

In the above section, the DoA-LF positioning algorithm with mmWave is proposed. In DoA-LF positioning algorithm, the number of APs, the interval of RPs, the channel model of mmWave and the error of DoA estimation have an impact on the positioning error. In this section, we analyze the impact of these parameters on positioning error, which can provide guideline for the selection of appropriate parameters in DoA-LF algorithm with mmWave.

As illustrated in Fig. 3, there are Q APs and M RPs. APs are distributed on the edge of a specific area denoted as area A . RPs are uniform distributed in area A . The location of test point is denoted as θ . DoA-LF algorithm generates the estimated point r with conditional probability $\Pr(r|\theta)$. The Euclidean distance between r and θ is $d_{r\theta}$. The conditional probability $\Pr(r|\theta)$ and the distance $d_{r\theta}$ can represent positioning error. Besides, $\Pr(r|\theta)$ is related with $d_{r\theta}$. In LF positioning, one-to-one mapping can be established between $2Q$ -dimensional feature space and two-dimensional geo-location space. Thus the expression of conditional probability $\Pr(r|\theta)$ in two-dimensional geo-location space equals to the conditional probability $\Pr(\mathbf{s}_r, \varphi_r | \mathbf{s}_\theta, \varphi_\theta)$ in $2Q$ -dimensional feature space, where $\mathbf{s}_\theta, \varphi_\theta, \mathbf{s}_r$ and φ_r are the RSSI and DoA information of all APs at location θ and r respectively. Therefore the conditional probability $\Pr(r|\theta)$ is as follows.

$$\begin{aligned} \Pr(r|\theta) &= \Pr(\mathbf{s}_r, \varphi_r | \mathbf{s}_\theta, \varphi_\theta) \\ &= \prod_{i=1}^Q \Pr(\mathbf{s}_{ir}, \varphi_{ir} | \mathbf{s}_{i\theta}, \varphi_{i\theta}) \\ &= \prod_{i=1}^Q \Pr(\mathbf{s}_{ir} | \mathbf{s}_{i\theta}) \prod_{i=1}^Q \Pr(\varphi_{ir} | \varphi_{i\theta}). \end{aligned} \quad (3)$$

The conditional probability $\Pr(\mathbf{s}_{ir} | \mathbf{s}_{i\theta})$ denotes that the actual signal strength of i th AP at the test point is $\mathbf{s}_{i\theta}$ while the received signal strength of i th AP is \mathbf{s}_{ir} , which is the signal strength at location r . $\Pr(\mathbf{s}_{ir} | \mathbf{s}_{i\theta})$ follows Gaussian distribution with mean $\mathbf{s}_{i\theta}$ and variance σ_s^2 [18][37]. Meanwhile, $\Pr(\varphi_{ir} | \varphi_{i\theta})$ denotes the conditional probability that the DoA of i th AP at test point is $\varphi_{i\theta}$ while the estimated DoA of i th AP is φ_{ir} , which is the DoA of i th AP at location r . $\Pr(\varphi_{ir} | \varphi_{i\theta})$ also follows Gaussian distribution with mean $\varphi_{i\theta}$ and variance σ_φ^2 [38][39].

According to the path loss model of mmWave in (1), assuming that the transmit power of each AP is P_t , the average signal strength at θ from i th AP is given by

$$s_{i\theta} = P_t - PL(d_{i\theta}) = P_t - PL(d_0) - 10n \log\left(\frac{d_{i\theta}}{d_0}\right) - X_\sigma, \quad (5)$$

where X_σ is a Gaussian random variable with mean zero and variance σ_s^2 . $d_{i\theta}$ is the distance between i th AP and the location θ .

CRLB is an effective tool to estimate the minimum variance of parameter estimation error [40][41][42]. In this subsection, the lower bound of the variance of DoA-LF algorithm error is analyzed by CRLB. Assuming that the test point is $\theta = (x, y)^T$, the unbiased estimation value of θ is $\hat{\theta} = (\hat{x}, \hat{y})^T$,

which is the weighted mean of K nearest RPs selected by DoA-LF algorithm. The covariance matrix of $\hat{\theta}$ is

$$\begin{aligned} \text{cov}(\hat{\theta}) &= E\left((\hat{\theta} - \theta)(\hat{\theta} - \theta)^T\right) \\ &= \begin{pmatrix} \text{var}(\hat{x} - x) & \text{cov}((\hat{x} - x), (\hat{y} - y)) \\ \text{cov}((\hat{y} - y), (\hat{x} - x)) & \text{var}(\hat{y} - y) \end{pmatrix}, \end{aligned} \quad (6)$$

where $E(\alpha)$ is the expectation of random variable α . $\text{var}(\alpha)$ is the variance of α . $\text{cov}(\alpha, \beta)$ is the covariance of random variables α and β . According to CRLB inequality, the covariance of $\hat{\theta}$ satisfies the following inequality [43][44].

$$\text{cov}(\hat{\theta}) \geq \left(J(\hat{\theta})\right)^{-1}, \quad (7)$$

where $J(\hat{\theta})$ is fisher information matrix (FIM), which is defined as follows [41][44].

$$J(\hat{\theta}) = E\left(-\frac{\partial^2 \ln f(r; \theta)}{\partial \theta \partial \theta^T}\right), \quad (8)$$

where r is the corresponding coordinates of $2Q$ -dimensional observation features and $f(r; \theta)$ is denoted as

$$f(r; \theta) = f(r|\theta)f(\theta). \quad (9)$$

According to one-to-one mapping relation between $2Q$ -dimensional feature space and two-dimensional geo-location space, the value of $f(r|\theta)$ is provided in (3). Besides, θ is uniformly distributed in area A , hence $f(\theta) = \frac{1}{|A|}$ where $|A|$ denotes the area of A . Thus the value of $f(r; \theta)$ is

$$\begin{aligned} f(r; \theta) &= \prod_{i=1}^Q \kappa \exp\left(-\frac{(s_{ir} - s_{i\theta})^2}{2\sigma_s^2} - \frac{(\varphi_{ir} - \varphi_{i\theta})^2}{2\sigma_\varphi^2}\right), \\ &= \prod_{i=1}^Q \kappa \exp\left(-\frac{\left(10n \lg\left(\frac{d_{ir}}{d_{i\theta}}\right)\right)^2}{2\sigma_s^2} - \frac{(\varphi_{ir} - \varphi_{i\theta})^2}{2\sigma_\varphi^2}\right), \end{aligned} \quad (10)$$

where $\kappa = \frac{1}{2\pi|A|\sigma_s\sigma_\varphi}$. d_{ir} is the distance between i th AP and the location r . $\lg(\ast)$ is a logarithmic function with base 10. Therefore the function $\log f(r; \theta)$ is as follows.

$$\begin{aligned} \log f(r; \theta) &= \sum_{i=1}^Q \log\left(\kappa \exp\left(-\frac{\left(10n \lg\left(\frac{d_{ir}}{d_{i\theta}}\right)\right)^2}{2\sigma_s^2} - \frac{(\varphi_{ir} - \varphi_{i\theta})^2}{2\sigma_\varphi^2}\right)\right) \\ &= \sum_{i=1}^Q \left(\log \kappa - \eta \left(\log\left(\frac{d_{ir}}{d_{i\theta}}\right)\right)^2 - \frac{(\varphi_{ir} - \varphi_{i\theta})^2}{2\sigma_\varphi^2}\right), \end{aligned} \quad (11)$$

where $\log(\ast)$ is a logarithmic function with base e . The value of η is

$$\eta = \left(\frac{10n}{\sqrt{2}\sigma_s \log 10}\right)^2. \quad (12)$$

It is noted that $d_{i\theta}$ and $\varphi_{i\theta}$ are functions of x and y , whose expressions are

$$\begin{aligned}
\frac{\partial^2 \log f(r; \theta)}{\partial x^2} &= \sum_{i=1}^Q \left(\frac{-2\eta \cos^2 \varphi_{i\theta}}{d_{i\theta}^2} + \eta \log\left(\frac{d_{ir}^2}{d_{i\theta}^2}\right) \frac{1 - 2\cos^2 \varphi_{i\theta}}{d_{i\theta}^2} - \frac{\sin^2 \varphi_{i\theta}}{\sigma_\varphi^2 d_{i\theta}^2} \right), \\
\frac{\partial^2 \log f(r; \theta)}{\partial x \partial y} &= \frac{\partial^2 \log f(r; \theta)}{\partial y \partial x} = \sum_{i=1}^Q \left(-\frac{\eta \sin 2\varphi_{i\theta}}{d_{i\theta}^2} - \eta \log\left(\frac{d_{ir}^2}{d_{i\theta}^2}\right) \frac{\sin 2\varphi_{i\theta}}{d_{i\theta}^2} + \frac{(\varphi_{ir} - \varphi_{i\theta}) \cos 2\varphi_{i\theta} - \cos \varphi_{i\theta} \sin \varphi_{i\theta}}{\sigma_\varphi^2 d_{i\theta}^2} \right), \\
\frac{\partial^2 \log f(r; \theta)}{\partial y^2} &= \sum_{i=1}^Q \left(\frac{-2\eta \sin^2 \varphi_{i\theta}}{d_{i\theta}^2} + \eta \log\left(\frac{d_{ir}^2}{d_{i\theta}^2}\right) \frac{1 - 2\sin^2 \varphi_{i\theta}}{d_{i\theta}^2} - \frac{\cos^2 \varphi_{i\theta}}{\sigma_\varphi^2 d_{i\theta}^2} \right).
\end{aligned} \tag{4}$$

$$\begin{aligned}
d_{i\theta} &= \sqrt{(x - x_i)^2 + (y - y_i)^2}, \\
\varphi_{i\theta} &= \arccos\left(\frac{x_i - x}{d_{i\theta}}\right) = \arcsin\left(\frac{y_i - y}{d_{i\theta}}\right),
\end{aligned} \tag{13}$$

which are illustrated by Fig. 4.

In order to obtain (8), we first derive the first order partial derivatives as follows.

$$\begin{aligned}
\frac{\partial \log f(r; \theta)}{\partial x} &= \sum_{i=1}^Q \eta \log\left(\frac{d_{ir}^2}{d_{i\theta}^2}\right) \frac{x - x_i}{d_{i\theta}^2} + \frac{(\varphi_{ir} - \varphi_{i\theta}) \sin \varphi_{i\theta}}{\sigma_\varphi^2 d_{i\theta}}, \\
\frac{\partial \log f(r; \theta)}{\partial y} &= \sum_{i=1}^Q \eta \log\left(\frac{d_{ir}^2}{d_{i\theta}^2}\right) \frac{y - y_i}{d_{i\theta}^2} + \frac{(\varphi_{ir} - \varphi_{i\theta}) \cos \varphi_{i\theta}}{\sigma_\varphi^2 d_{i\theta}}.
\end{aligned} \tag{14}$$

Then the second order derivatives can be derived, which are shown in (4).

For DoA-LF algorithm, d_{ir} approximately equals $d_{i\theta}$ and φ_{ir} approximately equals $\varphi_{i\theta}$. Hence the values of $\log\left(\frac{d_{ir}^2}{d_{i\theta}^2}\right)$ and $\varphi_{ir} - \varphi_{i\theta}$ approximate zero. The entries of (4) become as follows.

$$\begin{aligned}
\frac{\partial^2 \log f(r; \theta)}{\partial x^2} &= \sum_{i=1}^Q \left(-\frac{2\eta \cos^2 \varphi_{i\theta}}{d_{i\theta}^2} - \frac{\sin^2 \varphi_{i\theta}}{\sigma_\varphi^2 d_{i\theta}^2} \right), \\
\frac{\partial^2 \log f(r; \theta)}{\partial x \partial y} &= \frac{\partial^2 \log f(r; \theta)}{\partial y \partial x} \\
&= \sum_{i=1}^Q \left(-\frac{\eta \sin 2\varphi_{i\theta}}{d_{i\theta}^2} - \frac{\sin 2\varphi_{i\theta}}{2\sigma_\varphi^2 d_{i\theta}^2} \right), \\
\frac{\partial^2 \log f(r; \theta)}{\partial y^2} &= \sum_{i=1}^Q \left(-\frac{2\eta \sin^2 \varphi_{i\theta}}{d_{i\theta}^2} - \frac{\cos^2 \varphi_{i\theta}}{\sigma_\varphi^2 d_{i\theta}^2} \right).
\end{aligned} \tag{15}$$

Then the FIM $J(\hat{\theta})$ can be derived as follows.

$$J(\hat{\theta}) = \begin{pmatrix} J_{xx}(\hat{\theta}) & J_{xy}(\hat{\theta}) \\ J_{yx}(\hat{\theta}) & J_{yy}(\hat{\theta}) \end{pmatrix}, \tag{16}$$

where the entries of (16) are

$$\begin{aligned}
J_{xx}(\hat{\theta}) &= -\frac{\partial^2 \log f(r; \theta)}{\partial x^2} = \sum_{i=1}^Q \frac{2\eta \cos^2 \varphi_{i\theta}}{d_{i\theta}^2} + \frac{\sin^2 \varphi_{i\theta}}{\sigma_\varphi^2 d_{i\theta}^2}, \\
J_{xy}(\hat{\theta}) &= J_{yx}(\hat{\theta}) = \sum_{i=1}^Q \frac{\eta \sin 2\varphi_{i\theta}}{d_{i\theta}^2} + \frac{\sin 2\varphi_{i\theta}}{2\sigma_\varphi^2 d_{i\theta}^2}, \\
J_{yy}(\hat{\theta}) &= -\frac{\partial^2 \log f(r; \theta)}{\partial y^2} = \sum_{i=1}^Q \frac{2\eta \sin^2 \varphi_{i\theta}}{d_{i\theta}^2} + \frac{\cos^2 \varphi_{i\theta}}{\sigma_\varphi^2 d_{i\theta}^2}.
\end{aligned} \tag{17}$$

Therefore $(J(\hat{\theta}))^{-1}$ is

$$(J(\hat{\theta}))^{-1} = \frac{1}{|J(\hat{\theta})|} \begin{pmatrix} J_{yy}(\hat{\theta}) & -J_{yx}(\hat{\theta}) \\ -J_{xy}(\hat{\theta}) & J_{xx}(\hat{\theta}) \end{pmatrix}, \tag{18}$$

where $|J(\hat{\theta})|$ is

$$\begin{aligned}
|J(\hat{\theta})| &= J_{xx}(\hat{\theta})J_{yy}(\hat{\theta}) - J_{xy}(\hat{\theta})J_{yx}(\hat{\theta}) \\
&= \sum_{i=1}^Q \frac{2\eta(\cos^2 \varphi_{i\theta} - \sin^2 \varphi_{i\theta})^2}{\sigma_\varphi^2 d_{i\theta}^4}.
\end{aligned} \tag{19}$$

Substituting (6) and (18) into (7), we have

$$\begin{aligned}
&\begin{pmatrix} \text{var}(\hat{x} - x) & \text{cov}((\hat{x} - x), (\hat{y} - y)) \\ \text{cov}((\hat{y} - y), (\hat{x} - x)) & \text{var}(\hat{y} - y) \end{pmatrix} \\
&\geq \frac{1}{|J(\hat{\theta})|} \begin{pmatrix} J_{yy}(\hat{\theta}) & -J_{yx}(\hat{\theta}) \\ -J_{xy}(\hat{\theta}) & J_{xx}(\hat{\theta}) \end{pmatrix}.
\end{aligned} \tag{20}$$

Hence the CRLB $C_{\hat{\theta}}$ of positioning error is

$$\begin{aligned}
C_{\hat{\theta}} &= \text{var}(\hat{x} - x) + \text{var}(\hat{y} - y) \geq \frac{J_{xx}(\hat{\theta}) + J_{yy}(\hat{\theta})}{|J(\hat{\theta})|} \\
&= \sum_{i=1}^Q \frac{d_{i\theta}^2(1 + 2\eta\sigma_\varphi^2)}{2\eta(\cos^2 \varphi_{i\theta} - \sin^2 \varphi_{i\theta})^2}.
\end{aligned} \tag{21}$$

According to (21), CRLB is an increasing function of σ_φ^2 . Besides, CRLB is a decreasing function of η . Because of (12), we have conclusions as follows.

- 1) The variance of positioning error is increasing with the variance σ_s^2 , which means that the positioning error is increasing with the increase of shadow fading factor.
- 2) The variance of positioning error is decreasing with path loss exponent n , which means that LF positioning error

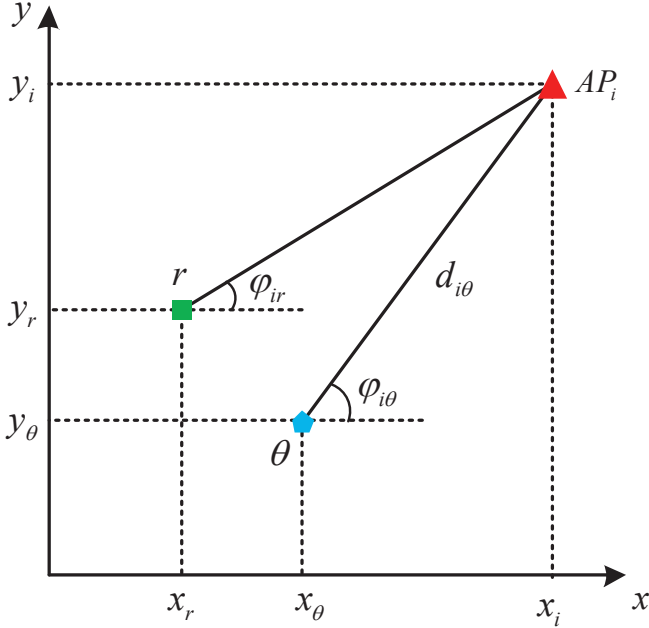


Fig. 4. The distance and DoA of θ and r .

can be reduced when using the signal with large path loss exponent, such as mmWave.

- 3) In LF positioning with mmWave, when σ_{φ}^2 is small, namely, the error of DoA estimation is small, the positioning error can be reduced.

Meanwhile, the variance of positioning error is also impacted by the interval of RPs and the number of APs. With the decreasing of the interval of RPs, the variance of positioning error is decreasing. However, when the interval is extremely small, the computational complexity of DoA-LF algorithm will be large. Besides, with the increasing of the number of APs, the positioning error can be reduced. However, when the number of APs is extremely large, the computational complexity of DoA-LF algorithm will be intolerable. Simulation results in Section V will support our analysis.

V. SIMULATION RESULTS AND ANALYSIS

A. DoA-LF Algorithm

Firstly, the LF positioning scheme with mmWave is compared with the traditional LF positioning with 2.4 GHz WiFi. The path loss models of 60 GHz mmWave and 2.4 GHz WiFi under the same indoor NLOS¹ environment are given as follows [27][28].

$$\begin{aligned} PL_{mmw}(d)[dB] &= -75.3 + 16.8 \log(d) + \mathcal{N}(0, 2.45), \\ PL_{2.4GHz}(d)[dB] &= -48.5 + 20.5 \log(d) + \mathcal{N}(0, 3.04). \end{aligned} \quad (22)$$

In order to create an offline database in the training phase, 100 samples of RSSI and DoA estimations at each RP are achieved. Then the average RSSI and DoA estimations at each RP are recorded in the offline database. The size of indoor environment is $100\text{m} \times 100\text{m}$ and RPs are deployed per 5

¹The LF positioning is mainly applied in the NLOS environment.

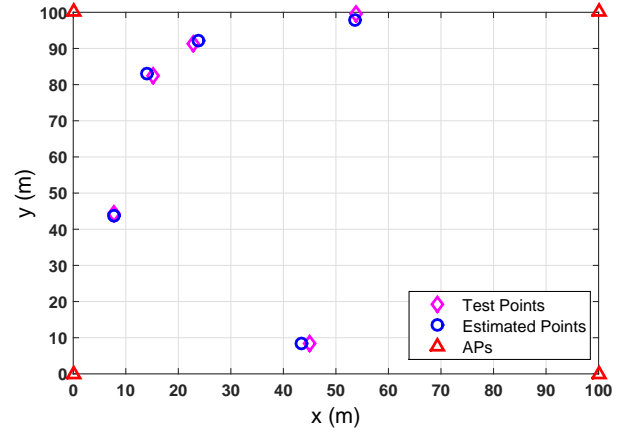


Fig. 5. A test of DoA-LF positioning algorithm.

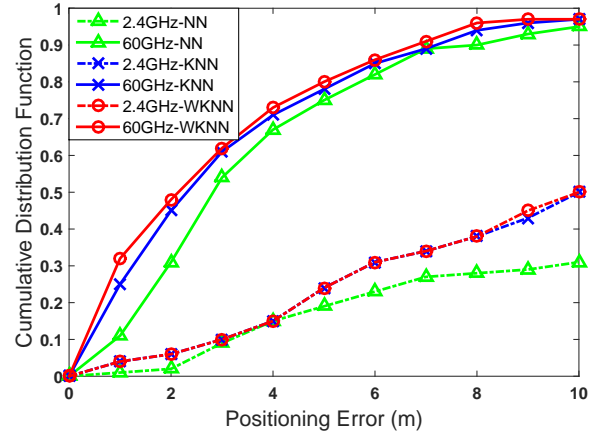


Fig. 6. Comparison of CDFs between 60 GHz mmWave and 2.4 GHz WiFi with different algorithms, where $K = 6$ for KNN and WKNN.

meters. Besides, 4 APs are distributed in the 4 corners of the entire region. The transmit power of each AP is 30 mW. Fig. 5 illustrates the intuitive results of DoA-LF algorithm, where the estimated points match the test points very well.

In order to present the errors of different positioning methods, the probability of successful positioning within the range of location error, namely, the cumulative distribution function (CDF) of LF positioning is simulated. Assume that the positioning error is E , which is a random variable. For any positioning error $E = e$ in the horizontal axis, its corresponding CDF, namely, the value in vertical axis is the probability of $E < e$. Besides, the average positioning errors of different methods are simulated.

Firstly, the impact of path loss models of 2.4 GHz WiFi and 60 GHz mmWave on three different LF positioning algorithms, namely, the algorithms of NN, KNN and WKNN, is illustrated in Fig. 6 and Fig. 7. In Fig. 6, the CDF curve of 60 GHz mmWave grows much faster than that of 2.4 GHz WiFi when using the same LF positioning algorithm². The underlying

²The proposed DoA-LF algorithm also adopts WKNN operations. However, in this section, the algorithms of nearest node (NN), K nearest node (KNN) and weight K nearest node (WKNN) denote the LF positioning algorithms without DoA estimation, namely, they only use RSSI information.

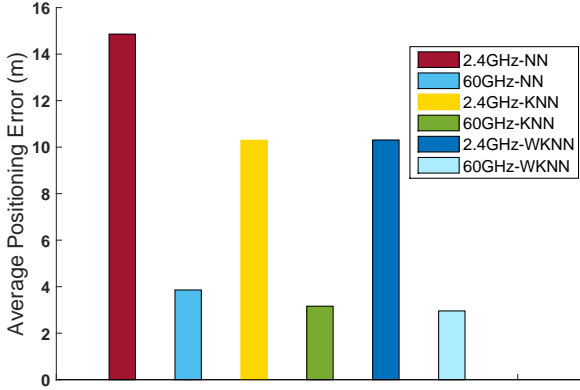


Fig. 7. Comparison of average positioning errors between 60 GHz mmWave and 2.4 GHz WiFi with different algorithms, where $K = 6$ for KNN and WKNN.

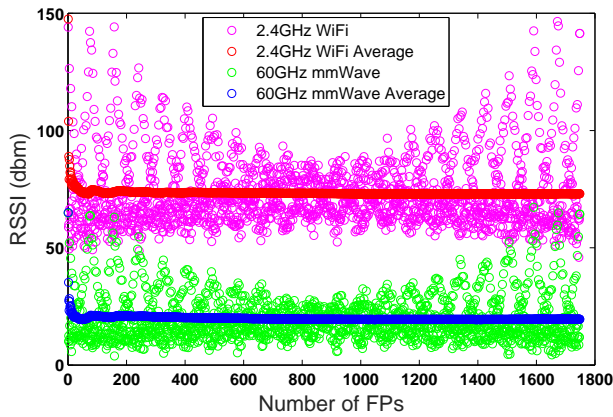


Fig. 8. Comparison of RSSI between 60 GHz mmWave and 2.4 GHz WiFi with the same transmit power of APs.

reason is that mmWave has the characteristics of narrow beam and fast attenuation, which can increase the discrimination of RSSI and DoA information of different RPs and reduce the positioning error. Besides, the positioning error of 60 GHz mmWave is much higher than that of 2.4 GHz WiFi when using the same LF positioning algorithm. Moreover, WKNN algorithm yields the lowest error and the fastest convergence speed among the three LF algorithms for 60 GHz mmWave. Fig. 7 shows that 60 GHz mmWave yields less positioning error compared with 2.4 GHz WiFi. The average positioning error of 60 GHz mmWave is 68.9% less than 2.4 GHz WiFi.

Fig. 8 illustrates the comparison of RSSI between 60 GHz mmWave and 2.4 GHz WiFi. In Fig. 8, the RSSI of 2.4 GHz WiFi is higher than that of 60 GHz mmWave at the same RP, which verifies the fact that the attenuation of 60 GHz mmWave signal is faster than that of 2.4 GHz signal. Besides, the distribution of RSSIs of mmWave signal is more concentrated compared with 2.4 GHz signal, which can increase the discrimination of RSSI to reduce positioning error.

Then we analyze the performance of the proposed DoA-LF algorithm which uses RSSI and DoA information for hybrid LF positioning with mmWave. The performance is compared

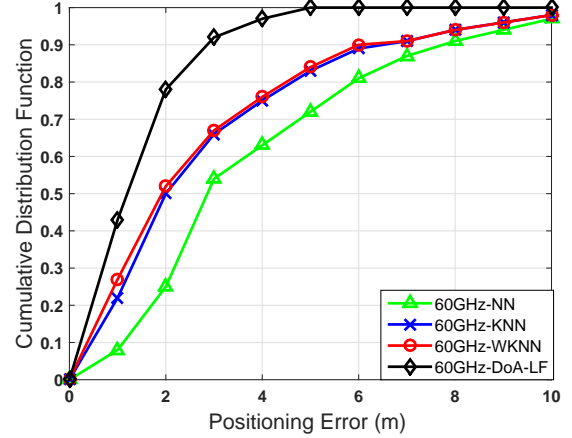


Fig. 9. Comparison of CDFs between DoA-LF algorithm and other algorithms in 60 GHz mmWave, where $K = 4$ for DoA-LF, KNN and WKNN.

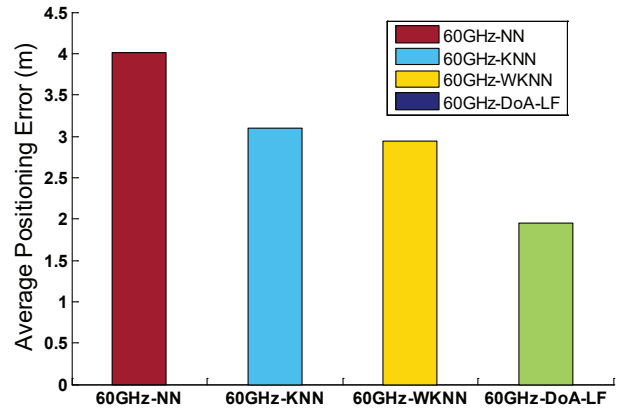


Fig. 10. Comparison of average positioning errors between DoA-LF algorithm and other algorithms in 60 GHz mmWave, where $K = 4$ for DoA-LF, KNN and WKNN.

with other three LF algorithms, which is illustrated in Fig. 9 and Fig. 10. Fig. 9 shows that the CDF curve of DoA-LF algorithm grows faster than other algorithms without DoA estimation, which means that the positioning error of DoA-LF algorithm is the lowest. Similarly, as illustrated in Fig. 10, DoA-LF algorithm yields less positioning error compared with other algorithms. The average positioning error of DoA-LF algorithm is 1.32 meters, which is approximately 50% less than WKNN and KNN algorithm without DoA estimation.

Finally, we compare the performance of DoA-LF algorithm with mmWave, WKNN algorithm with 60 GHz mmWave and WKNN algorithm with 2.4 GHz WiFi. As illustrated in Fig. 11, the positioning error of DoA-LF algorithm with 60 GHz mmWave is much lower than WKNN algorithm with 60 GHz mmWave and 2.4 GHz WiFi. As illustrated in Fig. 12, the average error distance of DoA-LF algorithm is 1.37 meters, which is 48.5% less than WKNN with 60 GHz mmWave and 85.6% less than WKNN with 2.4 GHz WiFi.

The relation between the average positioning error and K is illustrated in Fig. 13 to yield the optimal value of K in WKNN algorithm. It is noted that if K is small, the randomness is large

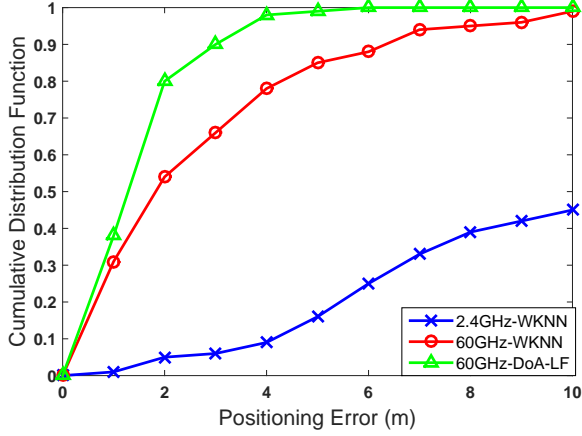


Fig. 11. Comparison of CDFs between DoA-LF with 60 GHz mmWave, WKNN with 60 GHz mmWave and WKNN with 2.4GHz WiFi, where $K = 6$ for DoA-LF and WKNN.

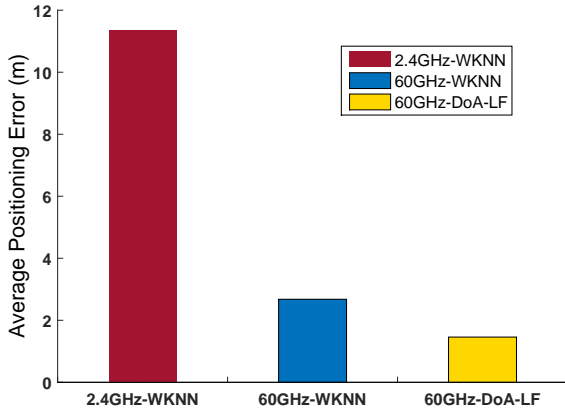


Fig. 12. Comparison of average positioning errors between DoA-LF with 60 GHz mmWave, WKNN with 60 GHz mmWave and WKNN with 2.4GHz WiFi, where $K = 6$ for DoA-LF and WKNN.

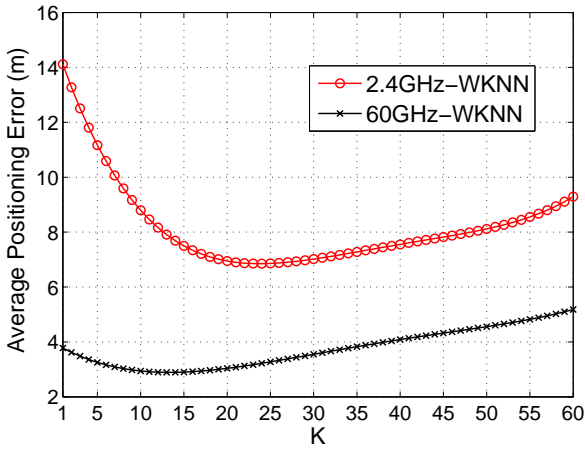


Fig. 13. The relation between the average positioning error and K .

and the average positioning error is large. On the contrary, if K is large, the disturbance from other RPs is correspondingly large and the average positioning error is also large. Thus there

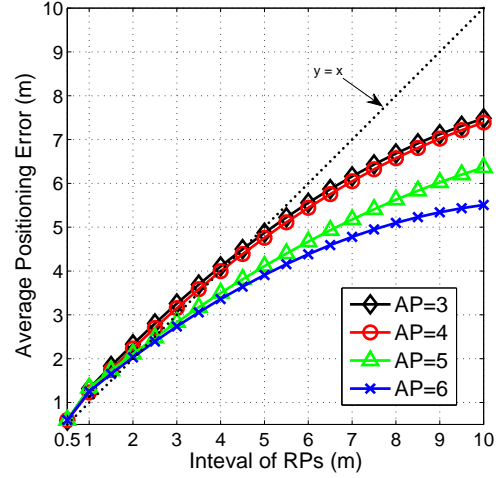


Fig. 14. The impact of the interval of RPs on average positioning error, where the number of APs varies from 3 to 6.

exists an optimal K to minimize the average positioning error, which is illustrated in Fig. 13. Besides, the average positioning error for any K with mmWave is still smaller than that with low frequency signal.

Overall, we have verified that the positioning error can be reduced significantly when employing DoA-LF positioning algorithm with mmWave.

B. CRLB and Analysis

In this subsection, the simulation results are shown to analyze the impact of various parameters on the average positioning error of DoA-LF algorithm, which include the number of APs, the interval of RPs, the path loss exponent, the DoA estimation error and the variance of received signal strength. These simulations and analysis can verify our analysis of CRLB in section IV. Besides, they can provide a guideline for the selection of appropriate parameters in the proposed DoA-LF positioning algorithm.

Firstly, we analyze the impact of the interval of RPs on average positioning error. Fig. 14 shows that the average positioning error is increasing with the increase of the interval of RPs. The curve $y = x$ is plotted in Fig. 14, where x denotes the interval of RPs and y denotes the average positioning error. It is noted that when the interval of RPs is too small, the average positioning error is larger than the interval of RPs, which is due to the fact that the CRLB has determined that the average positioning error cannot be as small as possible. Hence the interval of RPs does not have to be very small because the computational complexity of DoA-LF algorithm will be intolerable in this situation and the average positioning error is lower bounded by the CRLB. However, when the interval of RP is larger than a threshold, the average positioning error is smaller than the interval of RPs.

Then we analyze the impact of the number of APs on average positioning error. As illustrated in Fig. 15, the positioning error is decreasing with the increase of the number of APs. Since the increase of the number of APs will enlarge

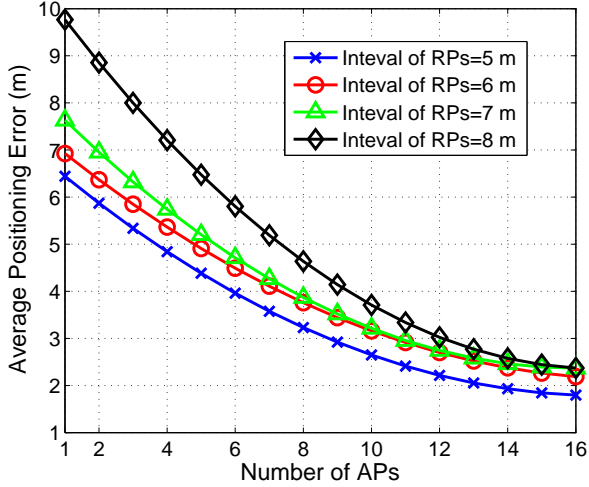


Fig. 15. The impact of the number of APs on average positioning error, where the interval of RPs varies from 5 to 8 meters.

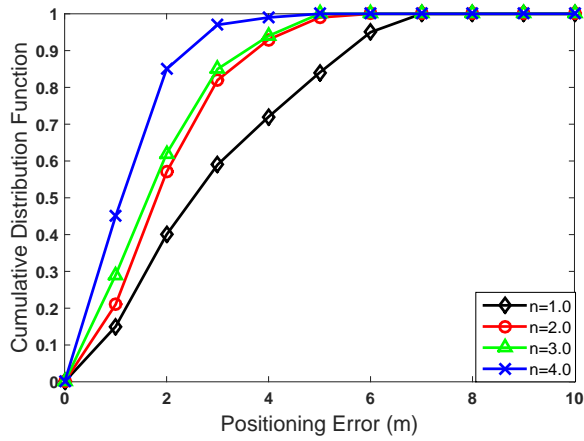


Fig. 16. The relation between positioning error and path loss exponent.

the computational complexity, there is an optimal number of APs in order to balance the computational complexity and positioning error.

Finally, we analyze the impact of the variance of DoA estimation, the path loss exponent and the variance of received signal strength on the average positioning error of DoA-LF algorithm with mmWave. In Fig. 16, the positioning error is decreasing with the increase of path loss exponent. In Fig. 17, the positioning error is decreasing with the decrease of the variance of received signal strength. In Fig. 18, the positioning error is decreasing with the decrease of the variance of DoA estimation. These results support our analysis results of CRLB in Section IV, which can be explained. When the path loss exponent is large, the discrimination of RSSI is correspondingly large, which can reduce positioning error. Besides, when the variance of signal intensity or DoA estimation is small, the fluctuation of RSSI or DoA estimation is correspondingly small, which can also reduce positioning error. However, the path loss exponent, the variance of received signal strength and the variance of DoA estimation are not controllable variables

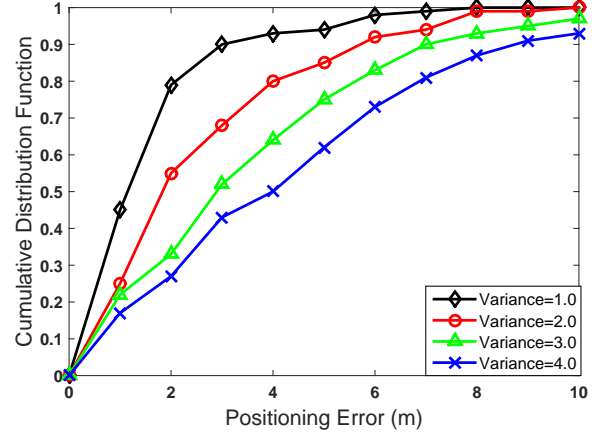


Fig. 17. The relation between positioning error and received signal strength variance.

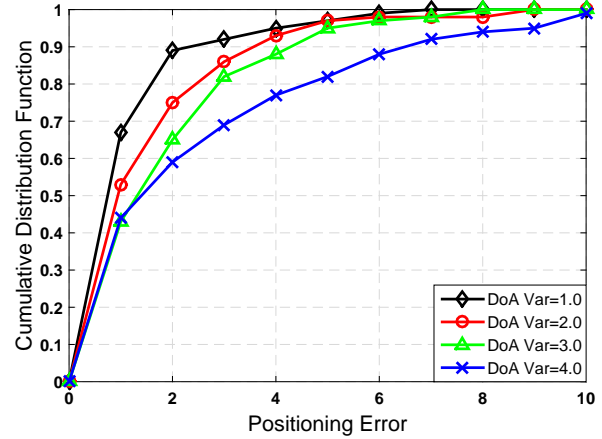


Fig. 18. The relation between positioning error and DoA estimation variance.

because they are impacted by the electromagnetic and physical environment. Therefore when the environment is not ideal, we can properly reduce the interval of RPs or increase the number of APs to bound positioning error.

VI. CONCLUSION

In this paper, the DoA-LF positioning algorithm is proposed, which incorporates the features of RSSI and DoA information into LF positioning. The characteristics of narrow beam and fast attenuation of mmWave are exploited to reduce positioning error. The DoA information obtained from MUSIC algorithm is combined with RSSI information to construct a joint offline database for online matching. Then the K candidate RPs with the most similar features are selected and their weighted mean is calculated, which is the estimated location. Moreover, the CRLB of DoA-LF positioning algorithm with mmWave is derived. Simulation results show that the positioning error of DoA-LF algorithm is much smaller than the algorithms without DoA estimation. Besides, the positioning error with mmWave is much smaller than that with low frequency signals. Moreover, we have shown that there exists an optimal K to minimize the positioning error via simulation. Finally, simulation results show that the positioning error is an increasing

function of the shadow fading factor, the interval of RPs and the error of DoA estimation. And the positioning error is a decreasing function of the path loss exponent and the number of APs. The study of this paper may provide guideline for indoor positioning in the era of 5G with densely deployed mmWave small cells.

ACKNOWLEDGMENT

The authors appreciate editor and anonymous reviewers for their precious time and great effort in improving this paper.

REFERENCES

- [1] S. He and S. H. G. Chan, "Wi-Fi Fingerprint-Based Indoor Positioning: Recent Advances and Comparisons," *IEEE Communications Surveys & Tutorials*, vol. 18, no. 1, pp. 466-490, Firstquarter 2016.
- [2] C. Steiner and A. Wittneben, "Low Complexity Location Fingerprinting With Generalized UWB Energy Detection Receivers," *IEEE Transactions on Signal Processing*, vol. 58, no. 3, pp. 1756-1767, Mar. 2010.
- [3] C. Steiner and A. Wittneben, "Efficient Training Phase for Ultrawideband-Based Location Fingerprinting Systems," *IEEE Transactions on Signal Processing*, vol. 59, no. 12, pp. 6021-6032, Dec. 2011.
- [4] R. Faragher and R. Harle, "Location Fingerprinting With Bluetooth Low Energy Beacons," *IEEE Journal on Selected Areas in Communications*, vol. 33, no. 11, pp. 2418-2428, Nov. 2015.
- [5] Y. Gu and F. Ren, "Energy-Efficient Indoor Localization of Smart Hand-Held Devices Using Bluetooth," *IEEE Access*, vol. 3, pp. 1450-1461, Jun. 2015.
- [6] Q. Jiang, Y. Ma, K. Liu and Z. Dou, "A Probabilistic Radio Map Construction Scheme for Crowdsourcing-Based Fingerprinting Localization," *IEEE Sensors Journal*, vol. 16, no. 10, pp. 3764-3774, May 2016.
- [7] S. H. Jung, B. C. Moon and D. Han, "Performance Evaluation of Radio Map Construction Methods for Wi-Fi Positioning Systems," *IEEE Transactions on Intelligent Transportation Systems*, vol. 18, no. 4, pp. 880-889, Apr. 2017.
- [8] S. He and S. H. G. Chan, "INTRI: Contour-Based Trilateration for Indoor Fingerprint-Based Localization," *IEEE Transactions on Mobile Computing*, vol. 16, no. 6, pp. 1676-1690, Jun. 2017.
- [9] Y. Shu, Y. Huang, J. Zhang, P. Coué, et al., "Gradient-Based Fingerprinting for Indoor Localization and Tracking," *IEEE Transactions on Industrial Electronics*, vol. 63, no. 4, pp. 2424-2433, Apr. 2016.
- [10] K. Wu, J. Xiao, Y. Yi, D. Chen, et al., "CSI-Based Indoor Localization," *IEEE Transactions on Parallel and Distributed Systems*, vol. 24, no. 7, pp. 1300-1309, Jul. 2013.
- [11] X. Wang, L. Gao and S. Mao, "CSI Phase Fingerprinting for Indoor Localization With a Deep Learning Approach," *IEEE Internet of Things Journal*, vol. 3, no. 6, pp. 1113-1123, Dec. 2016.
- [12] X. Wang, L. Gao, S. Mao and S. Pandey, "CSI-Based Fingerprinting for Indoor Localization: A Deep Learning Approach," *IEEE Transactions on Vehicular Technology*, vol. 66, no. 1, pp. 763-776, Jan. 2017.
- [13] S. Mahfouz, F. Mourad-Chehade, P. Honeine, J. Farah, et al., "Kernel-based machine learning using radio-fingerprints for localization in wsns," *IEEE Transactions on Aerospace and Electronic Systems*, vol. 51, no. 2, pp. 1324-1336, Apr. 2015.
- [14] H. Zou, B. Huang, X. Lu, H. Jiang, et al., "A Robust Indoor Positioning System Based on the Procrustes Analysis and Weighted Extreme Learning Machine," *IEEE Transactions on Wireless Communications*, vol. 15, no. 2, pp. 1252-1266, Feb. 2016.
- [15] X. Li, "RSS-Based Location Estimation with Unknown Pathloss Model," *IEEE Transactions on Wireless Communications*, vol. 5, no. 12, pp. 3626-3633, Dec. 2006.
- [16] U. Naik and V. N. Bapat, "Access Point Height Based Location Accuracy Characterization in LOS and OLOS Scenarios," *Wireless Personal Communications*, vol. 71, no. 3, pp. 2247-2258, Aug. 2013.
- [17] Y. Jin, W. S. Soh and W. C. Wong, "Error analysis for fingerprint-based localization," *IEEE Communications Letters*, vol. 14, no. 5, pp. 393-395, May 2010.
- [18] A. K. M. M. Hossain and W. S. Soh, "Cramer-Rao Bound Analysis of Localization Using Signal Strength Difference as Location Fingerprint," *IEEE International Conference on Computer Communications (INFOCOM)*, pp. 1-9, Mar. 2010.
- [19] A. M. Petroff, "Ultra Wideband Two-Way Time-of-Flight distance measurement Provides Sub-Centimeter range measurement accuracy," *USNC-URSI Radio Science Meeting (Joint with AP-S Symposium)*, pp. 212-212, Jul. 2015.
- [20] X. Cui, T. A. Gulliver, J. Li and H. Zhang, "Vehicle Positioning Using 5G Millimeter-Wave Systems," *IEEE Access*, vol. 4, pp. 6964-6973, Oct. 2016.
- [21] X. Cui, T. A. Gulliver, H. Song and J. Li, "Real-Time Positioning Based on Millimeter Wave Device to Device Communications," *IEEE Access*, vol. 4, pp. 5520-5530, Aug. 2016.
- [22] J. G. Andrews, S. Buzzi, W. Choi, S. V. Hanly, et al., "What Will 5G Be?," *IEEE Journal on Selected Areas in Communications*, vol. 32, no. 6, pp. 1065-1082, Jun. 2014.
- [23] T. Nitsche, C. Cordeiro, A. B. Flores, E. W. Knightly, et al., "IEEE 802.11ad: directional 60 GHz communication for multi-Gigabit-per-second Wi-Fi [Invited Paper]," *IEEE Communications Magazine*, vol. 52, no. 12, pp. 132-141, Dec. 2014.
- [24] W. Haiming, H. Wei, C. Jixin, S. Bo, et al., "IEEE 802.11aj (45GHz): A new very high throughput millimeter-wave WLAN system," *China Communications*, vol. 11, no. 6, pp. 51-62, Jun. 2014.
- [25] A. I. Sulyman, A. Alwarafy, H. E. Seleem, K. Humadi, et al., "Path Loss Channel Models for 5G Cellular Communications in Riyadh City at 60 GHz," *IEEE International Conference on Communication (ICC)*, pp. 1-6, May 2016.
- [26] T. S. Rappaport, R. W. Heath, Jr., R. C. Daniels, and J. N. Murdock, "Millimeter Wave Wireless Communications," *Pearson/Prentice Hall*, 2015.
- [27] N. Hakem, G. Delisle, Y. Coulibaly, "Radio-wave Propagation into an Underground Mine Environment at 2.4GHz, 5.8 GHz and 60 GHz," *European Conference on Antennas and Propagation (EuCAP)*, pp. 3592-3595, Apr. 2014.
- [28] P. F. M. Smulders, "Statistical Characterization of 60-GHz Indoor Radio Channels," *IEEE Transactions on Antennas and Propagation*, vol. 57, no. 10, pp. 2820-2829, Oct. 2009.
- [29] S. Geng, J. Kivinen, P. Vainikainen, "Propagation Characterization of Wideband Indoor Radio Channels at 60GHz," *IEEE International Symposium on Microwave, Antenna, Propagation and EMC Technologies for Wireless Communications*, vol. 1, pp. 314-317, Aug. 2005.
- [30] P. S. C. Thejaswi, K. Bynam, J. P. Nair, S. Jos, et al., "Low-complexity Direction Estimation Techniques for Fast Beamforming Training in Millimeter Wave Multiantenna Systems," *IEEE International Conference on Communication (ICC)*, pp. 1-6, May 2016.
- [31] D. H. Johnson, D. E. Dudgeon, "Array Signal Processing: Concepts and Techniques," *Prentice Hall*, Feb. 1993.
- [32] S. A. Dudani, "The Distance-Weighted k-Nearest-Neighbor Rule," *IEEE Transactions on Systems, Man, and Cybernetics*, vol. SMC-6, no. 4, pp. 325-327, Apr. 1976.
- [33] X. Ge and Z. Qu, "Optimization WIFI indoor positioning KNN algorithm location-based fingerprint," *IEEE International Conference on Software Engineering and Service Science (ICSESS)*, pp. 135-137, 2016.
- [34] S. H. Fang and T. N. Lin, "Indoor Location System Based on Discriminant-Adaptive Neural Network in IEEE 802.11 Environments," *IEEE Transactions on Neural Networks*, vol. 19, no. 11, pp. 1973-1978, Nov. 2008.
- [35] D. Wu, Y. Xu, L. Ma, "Research on RSS based Indoor Location Method," *Pacific-Asia Conference on Knowledge Engineering and Software Engineering*, pp. 205-208, Apr. 2009.
- [36] M. Zhang, S. Zhang, J. Cao, "Analysis and Simulation of Key Factors for Errors in WLAN-based Location Estimation," *Journal of System Simulation*, vol. 21, no. 15, pp. 4866-4870, Aug. 2009.
- [37] R. Berkvens, M. Weyn and H. Peremans, "Position error and entropy of probabilistic Wi-Fi fingerprinting in the UJIIndoorLoc dataset," *International Conference on Indoor Positioning and Indoor Navigation (IPIN)*, pp. 1-6, Oct. 2016.
- [38] P. Stoica, A. Nehorai, "MUSIC, maximum likelihood, and Cramer-Rao bound," *IEEE Transactions on Acoustics, Speech, and Signal Processing*, vol. 37, no. 15, pp. 720-741, Aug. 1989.
- [39] P. Stoica, A. Nehorai, "MUSIC, maximum likelihood, and Cramer-Rao bound: further results and comparisons," *IEEE Transactions on Acoustics, Speech, and Signal Processing*, vol. 38, no. 12, pp. 2140-2150, Aug. 1990.
- [40] Y. Shen, M. Z. Win, "Fundamental Limits of Wideband Localization - Part II: Cooperative Networks," *IEEE Transactions on Information Theory*, vol. 56, pp. 4981-5000, Sep. 2010.
- [41] G. Ding, Z. Tan, J. Wu, J. Zhang, "Efficient Indoor Fingerprinting Localization Technique Using Regional Propagation Model," *IEICE Transactions on Communication*, vol. E97B, no. 8, pp. 1728-1741, Aug. 2014.

- [42] I. Reuven and H. Messer, "A Barankin-type lower bound on the estimation error of a hybrid parameter vector," *IEEE Transactions on Information Theory*, vol. 43, no. 3, pp. 1084-1093, May 1997.
- [43] S. M. Kay, "Fundamentals of Statistical Signal Processing: Estimation Theory," *Prentice Hall*, 1993.
- [44] T. L. V. Trees, "Optimum Array Processing: Part IV of Detection, Estimation and Modulation Theory," *John Wiley & Sons*, 2002.